ELSEVIER

Journal of Luminescence 62 (1994) 77–84

JOURNAL OF LUMINESCENCE

Spectroscopy and crystal-field analysis for Nd^{3+} in $GdLiF_4$

Frederick G. Anderson[a], H. Weidner[b], P.L. Summers[b], R.E. Peale[b,*]

[a]*Department of Physics, University of Vermont, Burlington, VT 05405, USA*
[b]*Department of Physics, University of Central Florida, Orlando, FL 32816, USA*

Received 5 August 1993; revised 2 November 1993; accepted 21 February 1994

Abstract

Spectroscopic results are presented and crystal-field parameters are determined for Nd^{3+} in the new laser crystal $GdLiF_4$. We take the unusual approach of expanding the crystal field in terms of operators transforming as irreducible representations of the T_d group. This allows us to directly interpret the parameters in terms of a point-charge structural model. The traditional B_{kq} parameters are then obtained via a linear transformation. Their values are nearly identical to those for Nd^{3+} in $YLiF_4$. The slightly weaker crystal field for $GdLiF_4$ suggests a dilation of the lattice caused by the larger ionic size of Gd^{3+} as compared to Y^{3+}.

1. Introduction

Renewed interest in insulating crystals activated with Nd^{3+} ions for lasing at 1 μm is based in part on the development of powerful AlGaAs diode lasers, whose emission matches a strong Nd^{3+} absorption band at about 0.8 μm. This has led to many innovative schemes for compact, all solid state, optically pumped, Nd lasers [1]. Microchip fabrication is a future possibility. For efficient operation, the active medium must absorb a significant fraction of the pump energy. This fraction decreases with the dimensions of the medium, so it is worthwhile to seek host–dopant combinations with increased absorption strength. One solution is to find a crystal which can be doped to high concentrations without sacrificing other desirable properties such as high emission cross section and long excited-state lifetimes.

With this motivation, a new crystal, in which Gd^{3+} is substituted for Y^{3+} in $YLiF_4$ (YLF), has been developed recently [2,3]. (YLF is a well known and commercially available crystal.) The key idea is that the Gd^{3+} ion is closer in size to Nd^{3+} than is Y^{3+}, permitting potentially higher doping levels. Integrated absorption versus nominal Nd^{3+} concentration reveals enhanced actual doping levels in $GdLiF_4$ (GLF) while lasing characteristics remain excellent [2,3]. The near identity in number, relative strength, polarization, and frequency position of Nd^{3+} spectral lines in GLF and YLF strongly suggests that the two crystals are isostructural [2–4]. A corresponding similarity in Raman spectra supports this idea [5].

One purpose of this paper is to report a calculation of crystal-field parameters from accurate levels determined for Nd^{3+} in GLF by

* Corresponding author.

SSDI 0022-2313(94)00018-8

Fourier-transform spectroscopy. By comparing these values with those determined by us for YLF, we are able to present a quantitative discussion of the small but measurable differences in the two crystals.

A second purpose is to present and discuss a new method of parameterizing the crystal field, in which the crystal-field Hamiltonian is expanded in a cubic basis rather than the usual spherical one. An advantage of this method is that the resulting fitting parameters are much easier to interpret in terms of the crystal structure at the dopant site than are the traditional parameters.

2. Experiment

The two GLF samples studied here were cut from single-crystal boules grown by the top-seeded solution growth method (modified Czochralski technique) at the Center for Research and Education in Optics and Lasers (CREOL) crystal-growth facility. The Nd^{3+} concentrations in the melt were 1.3 and 2.5 at.%. The actual Nd^{3+} concentrations in the grown crystals are estimated to be 1.0 and 2.0 at.%, respectively, since the distribution coefficient of Nd^{3+} in GLF is about 0.8. The samples are 5.6 and 2.1 mm thick, respectively. The YLF samples studied here were also grown at CREOL.

A Bomem DA8 Fourier-transform spectrometer collected both absorption and photoluminescence data, the latter excited by a multiline Ar laser. A variety of resources were used with the spectrometer: The beamsplitter was either quartz or Ge-coated KBr; the detector, HgCdTe or InSb operating at 77 K or a room-temperature Si photodiode. The frequency accuracy of the instrument is 0.004 cm^{-1} at 2000 cm^{-1}. A resolution of 1 cm^{-1} was sufficient to resolve all lines. Peak positions are determined interactively using a high-resolution graphics monitor and the uncertainty in the values is less than 0.5 cm^{-1} in most cases. The entire light path is in vacuum, so positions of absorption and luminescence peaks are in vacuum wavenumbers. All the spectra presented here were collected at 80 K sample temperatures using a home built liquid-nitrogen cold-finger cryostat. The

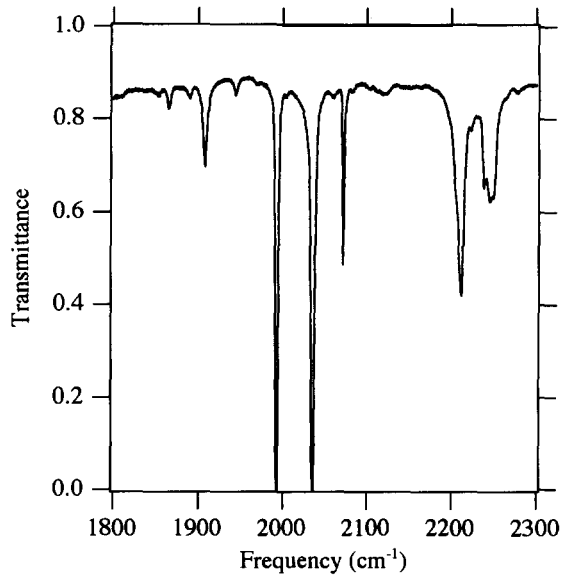

Fig. 1. $^4I_{9/2} \rightarrow {}^4I_{11/2}$ transmission spectrum for Nd^{3+} in $GdLiF_4$.

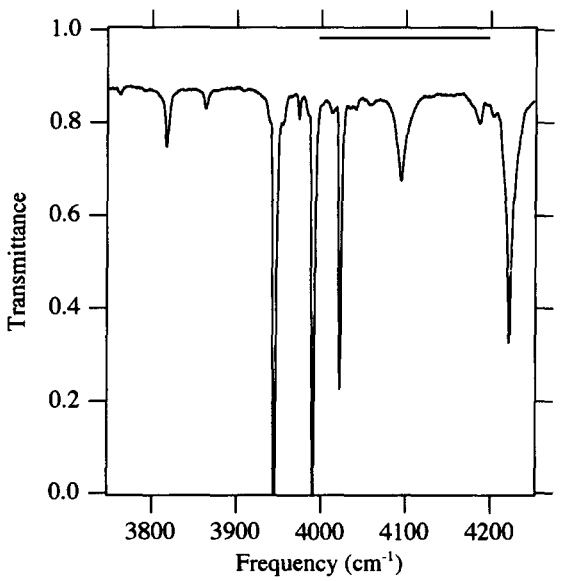

Fig. 2. $^4I_{9/2} \rightarrow {}^4I_{13/2}$ transmission spectrum for Nd^{3+} in $GdLiF_4$.

polarization chosen was σ because more transitions are observed than in π.

Figs. 1–3 present the $^4I_{9/2} \rightarrow {}^4I_{11/2}$, $^4I_{13/2}$, and $^4I_{15/2}$ transitions in the 1.3 at.% sample. The

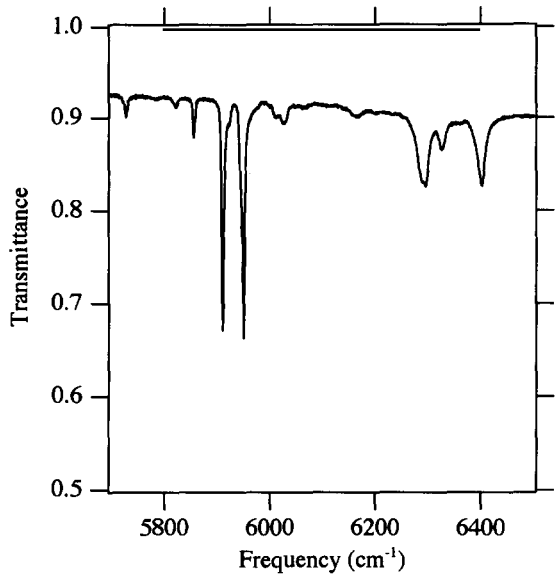

Fig. 3. $^4I_{9/2} \rightarrow {}^4I_{15/2}$ transmission spectrum for Nd^{3+} in $GdLiF_4$.

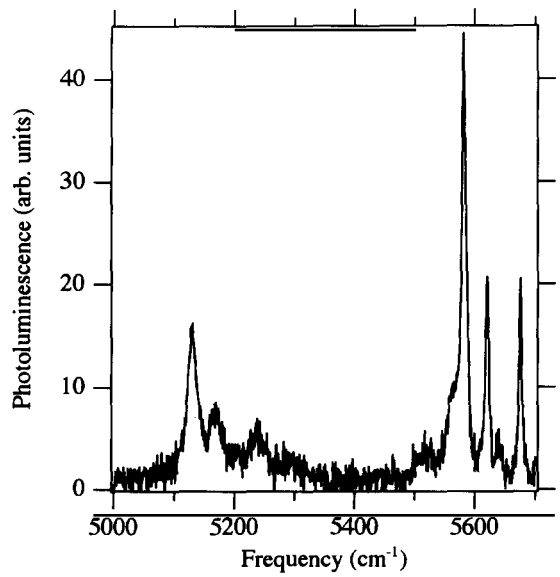

Fig. 4. $^4F_{3/2} \rightarrow {}^4I_{15/2}$ photoluminescence spectrum for Nd^{3+} in $GdLiF_4$.

$^4F_{3/2} \rightarrow {}^4I_{15/2}$ and $^4I_{13/2}$ photoluminescence bands of the 2.5 at.% sample are presented in Figs. 4 and 5, and the $^4F_{3/2} \rightarrow {}^4I_{11/2}$, $^4I_{9/2}$ bands for the 1.3 at.% crystal are presented in Figs. 6 and 7.

Table 1
Stark levels (cm^{-1}) of the ^4I J-multiplets for Nd^{3+} in $GdLiF_4$

J-multiplet	Experimental	Calculated
$^4I_{9/2}$	0	0
	128.0	132.2
	182.0	184.9
	239.0	249.6
	496.0	511.5
$^4I_{11/2}$	1992.7	1992.0
		2031.6
	2036.4	2035.1
	2071.8	2072.1
	2211.4	2211.1
	2247.0	2246.5
$^4I_{13/2}$	3944.3	3941.0
	3973.7	3969.8
	3990.3	3985.5
	4021.9	4019.9
	4186.6	4188.9
	4202.6	4209.0
	4221.8	4216.3
$^4I_{15/2}$	5855.5	5857.4
	5911.0	5919.0
	5949.7	5951.4
	6025.2	6029.2
	6295.2	6284.6
	6326.7	6323.6
	6366.0	6356.5
	6401.4	6402.2

Spectroscopy was also performed on a 5 at.% sample. Only very slight differences in linewidths and no difference in center frequencies were observed for the different concentrations.

From the photoluminescence and absorption lines, we obtain the Stark levels for the ^4I J-multiplets of Nd^{3+} in GLF at 80 K. These data are presented in Table 1. The two levels of $^4F_{3/2}$ used in the analysis of the photoluminescence spectra were 11 530.9 and 11 588.7 cm^{-1}. No Stokes shifts between absorption and emission values and no shifts with concentration were observed within the experimental uncertainty. The values in Table 1 are averages of absorption and emission data for all samples measured. Many absorption transitions originating in the first two excited levels of the $^4I_{9/2}$ manifold, which are thermally populated at 80 K, were observed and also used in the analysis.

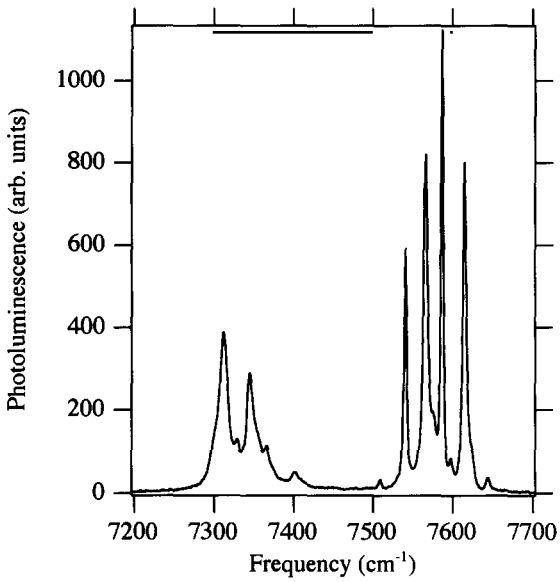

Fig. 5. $^4F_{3/2} \rightarrow {}^4I_{13/2}$ photoluminescence spectrum for Nd^{3+} in $GdLiF_4$.

For comparison, our own determination of the corresponding levels in Nd^{3+}:YLF are presented in Table 2. The $^4F_{3/2}$ levels used here were found to be 11 535.7 and 11 594.5 cm^{-1}. It is clear that the levels in Tables 1 and 2 are very similar for the two crystals. Together with the near identity in number, position, polarization, and relative strengths of spectral lines in both absorption and photoluminescence [3,4], we take GLF to be isostructural with YLF. This conclusion is the starting point for the theoretical comparison presented next.

3. Crystal-field model

Here we develop a crystal field model for the electronic structure of Nd^{3+} (f^3 configuration) substituting for Gd^{3+} in GLF or for Y^{3+} in YLF. According to Hund's rules, the ground term is ^4I, to which we confine our study. The spin–orbit interaction dominates over the crystal-field interaction and splits the ^4I term into manifolds of $J = 9/2$ (the ground manifold), $J = 11/2$, $J = 13/2$, $J = 15/2$. These manifolds interact with manifolds of the same J within excited terms. We account for this mixing in determining corrections to the Landé interval rule for the relative energy positions of the ^4I-term J-manifolds. However, our calculation of the crystal-field matrix elements between states of the ^4I term ignores this spin–orbit mixing with higher energy terms, as only the ^4I state wave functions are used. The level of this approximation is identical to that of Karayianis in Ref. [7].

Table 2
Stark levels (cm^{-1}) of the ^4I J-multiplets for Nd^{3+} in $YLiF_4$

J-multiplet	Experimental	Calculated
$^4I_{9/2}$	0	0
	132.1	135.8
	182.5	180.5
	247.2	257.6
	526.6	537.5
$^4I_{11/2}$	1997.1	1995.7
	2040.1	2035.5
	2042.4	2042.1
	2077.0	2076.0
	2226.8	2227.7
	2261.9	2264.5
$^4I_{13/2}$	3947.2	3944.1
	3975.9	3973.1
	3993.9	3989.6
	4023.5	4022.1
	4204.4	4210.1
	4214.3	4223.3
	4239.5	4233.4
$^4I_{15/2}$	5848.5	5852.5
	5909.5	5919.8
	5944.9	5947.8
	6031.5	6031.7
	6312.6	6303.6
	6346.1	6343.0
	6390	6379.9
	6431.8	6432.4

To motivate our theoretical approach and give background necessary for discussing our fitting parameters, we describe the local environment of Nd^{3+} in YLF. The Nd^{3+} sits in a low symmetry crystal-field which splits the J-multiplets, leaving only two-fold Kramers degeneracy. Recent crystallography by Goryunov and Popov [6] fully determined the symmetry at the Y^{3+} (Nd^{3+}) site, which is surrounded by eight F^- ions. These ions form two tetragonally distorted tetrahedra, as shown in Fig. 8 with the distortions exaggerated for clarity. The ions of the nearest neighbor tetrahedron ADEH ($c/a = 0.597$) are 2.247 Å from the Nd^{3+}.

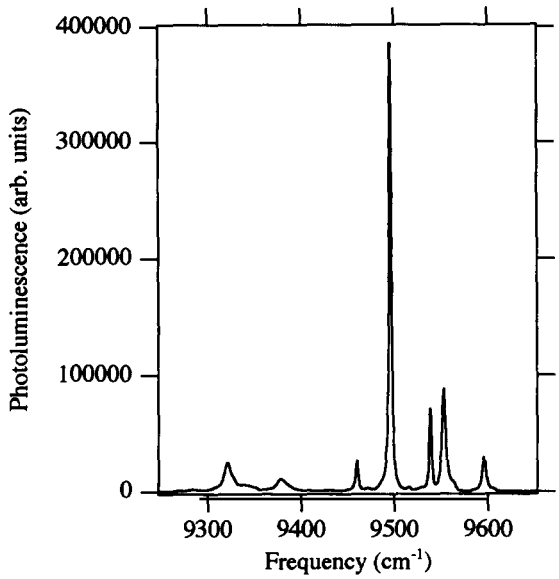

Fig. 6. $^4F_{3/2} \rightarrow {}^4I_{11/2}$ photoluminescence spectrum for Nd^{3+} in $GdLiF_4$.

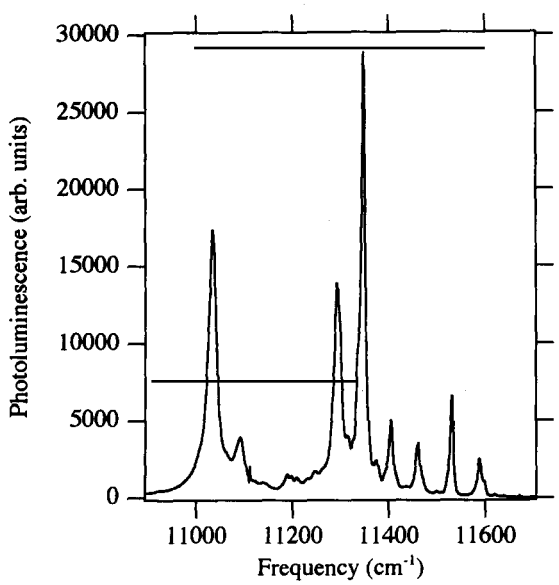

Fig. 7. $^4F_{3/2} \rightarrow {}^4I_{9/2}$ photoluminescence spectrum for Nd^{3+} in $GdLiF_4$.

The second nearest neighbor tetrahedron BCFG ($c/a = 1.813$) is a distance 2.299 Å from the Nd^{3+}. The c axes of these two tetrahedra are aligned with that of the crystal, but their x and y axes are rotated

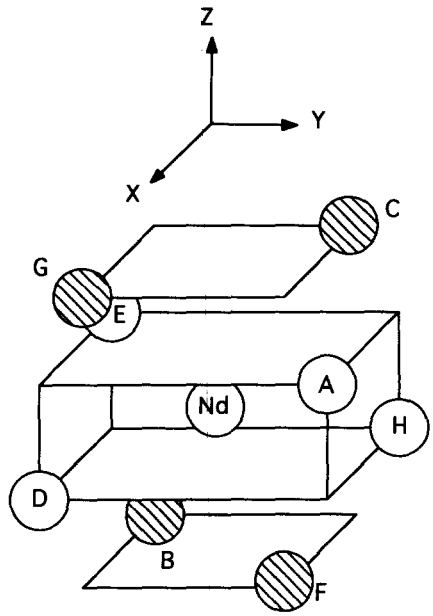

Fig. 8. The eight F^- neighbors to the Nd^{3+} dopant ion in $YLiF_4$. These eight F^- ions form two tetragonally distorted tetrahedra. The nearest neighbor tetrahedron (ADEH) is shown by the open ions, and the second neighbor tetrahedron (BCFG) by hatched ions.

with respect to the crystal axes. Finally, the two tetrahedrons are imperfectly aligned with each other: Segment AE makes an angle of 86.1° with segment GC. The deviation from 90° makes the actual site symmetry S_4. Since the deviation is small, we assume D_{2d} symmetry in our model. This is consistent with several previous determinations [7–12] of crystal-field parameters in YLF that have shown that the matrix elements resulting from reducing the symmetry to S_4 are relatively small.

Traditionally, the crystal-field parameters reported for YLF have been the B_{kq} that are real-valued coefficients associated with operators (C_{kq}) transforming as the kqth spherical harmonic. The corresponding Hamiltonian for an f electron in D_{2d} symmetry is

$$H_{cf} = B_{20}C_{20} + B_{40}C_{40} + B_{60}C_{60} + B_{44}(C_4 + C_{4,-4}) + B_{64}(C_{64} + C_{6,-4}). \quad (1)$$

While this form simplifies computations, the B_{kq} are difficult to interpret. With the motivation of Fig. 8, we use instead a crystal-field Hamiltonian whose

operators transform as the irreducible representations of the tetrahedral group T_d.

The f states span the irreducible representations a_1, t_2, and t_1 of the T_d group. The combinations of the $l = 3$ spherical harmonics that make up the states of these representations are

$$|a_1\rangle = \frac{-i}{\sqrt{2}}|3,-2\rangle + \frac{i}{\sqrt{2}}|3,2\rangle \sim xyz,$$

$$|t_{2\xi}\rangle = \frac{\sqrt{5}}{4}|3,-3\rangle - \frac{\sqrt{3}}{4}|3,-1\rangle + \frac{\sqrt{3}}{4}|3,1\rangle - \frac{\sqrt{5}}{4}|3,3\rangle \sim (5x^2 - 3r^2)x,$$

$$|t_{2\eta}\rangle = -\frac{i\sqrt{5}}{4}|3,-3\rangle - \frac{i\sqrt{3}}{4}|3,-1\rangle - \frac{i\sqrt{3}}{4}|3,1\rangle - \frac{i\sqrt{5}}{4}|3,3\rangle \sim (5y^2 - 3r^2)y,$$

$$|t_{2\zeta}\rangle = |3,0\rangle \sim (5z^2 - 3r^2)z.$$

$$|t_{1x}\rangle = -\frac{\sqrt{3}}{4}|3,-3\rangle - \frac{\sqrt{5}}{4}|3,-1\rangle + \frac{\sqrt{5}}{4}|3,1\rangle + \frac{\sqrt{3}}{4}|3,3\rangle \sim (y^2 - z^2)x,$$

$$|t_{1y}\rangle = -\frac{i\sqrt{3}}{4}|3,-3\rangle + \frac{i\sqrt{5}}{4}|3,-1\rangle + \frac{i\sqrt{5}}{4}|3,1\rangle - \frac{i\sqrt{3}}{4}|3,3\rangle \sim (z^2 - x^2)y,$$

$$|t_{1z}\rangle = \frac{1}{\sqrt{2}}|3,-2\rangle + \frac{1}{\sqrt{2}}|3,2\rangle \sim (x^2 - y^2)z. \quad (2)$$

In Eq. (2) x, y, and z are the cubic axes for the YF_4 tetrahedra in Fig. 8. Only z is parallel to one of the crystal axes (c).

Within this basis, the one-electron crystal-field Hamiltonian for D_{2d} symmetry is

$$H_{cf} = \begin{pmatrix} -3(\beta+\gamma) & 0 & 0 & 0 & 0 & 0 & 0 \\ 0 & \beta - B/2 & 0 & 0 & -Y & 0 & 0 \\ 0 & 0 & \beta - B/2 & 0 & 0 & Y & 0 \\ 0 & 0 & 0 & \beta + B & 0 & 0 & 0 \\ 0 & -Y & 0 & 0 & \gamma - C/2 & 0 & 0 \\ 0 & 0 & Y & 0 & 0 & \gamma - C/2 & 0 \\ 0 & 0 & 0 & 0 & 0 & 0 & \gamma + C \end{pmatrix}. \quad (3)$$

The parameters β and γ give the splitting of the f states into a singlet a_1, and two triplets t_2 and t_1 by a perfect tetrahedral field. The tetragonal distortions along $z(c)$, giving D_{2d} symmetry, split each triplet into a doublet and a singlet: the $t_{2\zeta}$ and t_{1z} states are split off as described by the parameters B and C. Finally, the D_{2d} crystal field mixes t_{1x} with $t_{2\xi}$ and mixes t_{1y} with $t_{2\eta}$, as given by the parameter Y. Having described the crystal-field in terms of one-electron crystal-field parameters, we then calculate, in terms of these parameters, the many-electron matrix elements between the states of the ^4I term. The energy positions of the various Stark levels are the result of simultaneously diagonalizing the spin–orbit and crystal-field interactions. A straightforward linear transformation converts our β, γ, B, C, and Y into the B_{kq} for comparison with the previous results.

4. Results and discussion

We have performed a least squares fit to our experimental levels for Nd^{3+} in GLF (Table 1) and in YLF (Table 2). The energy positions of the $^4I_{11/2}$, $^4I_{13/2}$, and $^4I_{15/2}$ manifolds relative to the $^4I_{9/2}$ manifold were varied in addition to β, γ, B, C, and Y, giving eight independent parameters to fit more than twenty levels. Results are given in Tables 3 and 4 for GLF and YLF, respectively. Levels calculated using these results are given next to the experimental values in Tables 1 and 2. For each crystal, the rms deviation is less than 6 cm^{-1}, which shows that our fit is rather good.

The energy positions of the excited spin–orbit manifolds are identical in GLF and YLF, another demonstration of the similarity of these two hosts. The crystal-field parameters for the two hosts differ only slightly, but on average the GLF parameters

Table 3
Crystal-field parameters and J-multiplet positions for Nd^{3+} in $GdLiF_4$

Crystal-field parameters [cm^{-1}]		J-multiplet positions [cm^{-1}]
$\beta = -124$	$B_{20} = 475$	
$\gamma = -115$	$B_{40} = -916$	$E(^4I_{11/2}) = 1864$
$B = 72.7$	$B_{60} = -48.3$	$E(^4I_{13/2}) = 3838$
$C = -219$	$B_{44} = -1050$	$E(^4I_{15/2}) = 5890$
$Y = -143$	$B_{64} = -988$	

Table 4
Crystal-field parameters and J-multiplet positions for Nd^{3+} in $YLiF_4$

Crystal-field parameters [cm^{-1}]		J-multiplet positions [cm^{-1}]
$\beta = -127$	$B_{20} = 482$	
$\gamma = -126$	$B_{40} = -982$	$E(^4I_{11/2}) = 1864$
$B = 68.3$	$B_{60} = -35.4$	$E(^4I_{13/2}) = 3838$
$C = -219$	$B_{44} = -1079$	$E(^4I_{15/2}) = 5890$
$Y = -148$	$B_{64} = -1058$	

are slightly smaller than those for YLF. This is simply explained by considering that Gd^{3+} has a larger ionic radius than Y^{3+} [13]. Thus, for GLF we expect larger lattice constants, larger separation between the Nd^{3+} ion and its neighbors, and therefore a weaker crystal-field interaction.

Our crystal-field parameters can be interpreted in terms of the one-electron wave functions (Eq. (2)) and the positions of the anion neighbors (Fig. 8). We neglect the Li^+ and $Y^{3+}(Gd^{3+})$ ions because these are farther away from the Nd^{3+} and are presumed to be well-screened by their F^- cages. The a_1 state has eight lobes directed along the $\langle 111 \rangle$ directions, where negatively-charged F^- ions lie, giving a_1 high energy. In contrast, the t_2 states have large lobes along the associated cubic axes, e.g. $t_{2\zeta}$ has its lobes along z. These lobes run between the F^- ions, making the t_2 states energetically favorable. Between these extremes, the t_1 states possess eight lobes located in the planes formed by the cubic axes but not along the axes themselves. For example, t_{1z} has four lobes in the xz plane and four lobes in the yz plane. All eight lobes are tilted away from the xy plane by $\pm 35°$, bringing the t_1 lobes closer to the anions, and thereby increasing the energy of t_1 relative to t_2. These simple arguments explain the negative signs and relative sizes of β and γ.

Consider now the tetragonal distortions of the two YF_4 tetrahedra. For the elongated one (BCFG), the F^- ions are 1.46 times closer to the z axis than they are to either x or y. For the flattened one (ADEH), the F^- ions are only 1.21 times closer to x or y than they are from z. Thus, the elongated tetrahedron should contribute more to the symmetry lowering field. Working against this idea, BCFG is slightly more distant from the Nd^{3+} than is ADEH, though this amounts to only a 2% difference. We argue that the significantly greater distortion overcomes the effect of being slightly more distant. Hence, both distortions together give effectively a single tetragonal distortion with $c/a > 1$. In such a distortion, the anions are closer to the z axis, increasing the energy of the state $t_{2\zeta}$ (with its lobes along z), i.e. B is positive. By the same token, the energy of the t_{1z} state (with lobes slightly tilted from the xy plane) is reduced, i.e. C is negative. The signs of off-diagonal matrix elements are difficult to interpret from a simple point-ion model, and we make no attempt to interpret Y.

In summary, we have presented spectroscopic data and the energy levels determined from them for Nd^{3+} in the new crystal $GdLiF_4$. We fit a crystal-field Hamiltonian to our data and find that both $GdLiF_4$ and $YLiF_4$ have very similar fitting parameters, indicating only slight differences in the crystal field at the Nd^{3+} site between these two crystals. We interpret our parameters in terms of the interaction between Nd^{3+} orbitals and the nearest neighbor F^- ions for the recently determined structure of $YLiF_4$. A slightly weaker crystal field for $GdLiF_4$ can be explained by a lattice dilation caused by the larger ionic size of Gd^{3+} compared to Y^{3+}.

Acknowledgements

The authors are very grateful for the generous assistance of Prof. Bruce Chai in providing the crystals used in this research.

References

[1] A.A. Pinto and T.Y. Fan (eds.), OSA Proc. on Advanced Solid-State Lasers, Vol 15 (Optical Society of America, Washington DC, 1993) pp. 2–108.
[2] X.X. Zhang, M. Bass, A.B. Villaverde, J. Lefaucheur, A. Pham and B.H.T. Chai, Appl. Phys, Lett. **62** (1993) 1197.
[3] X.X. Zhang, A.B. Villaverde, M. Bass, B.H.T. Chai, H. Weidner, R.I. Ramotar and R.E. Peale, J. Appl. Phys. **74** (1993) 790.
[4] H. Weidner, R.E. Peale, X.X. Zhang, M. Bass and B.H.T. Chai, in: OSA Proc. on Advanced Solid-State Lasers, Vol. 15, eds. A.A. Pinto and T.Y. Fan (Optical Society of America, Washington, DC, 1993) pp. 55–58.
[5] X.X. Zhang, A. Schulte and B.H.T. Chai, Solid State Commun. 89 (1994) 181.
[6] A.V. Goryunov and A.I. Popov, Russ. J. Inorg. Chem. **37** (1992) 126.
[7] N. Karayianis, J. Phys. Chem. Solids **32** (1971) 2385.
[8] D.E. Wortman, J. Phys. Chem. Solids **33** (1972) 311.
[9] A.A.S. da Gama, G.F. de Sá, P. Porcher and P. Caro, J. Chem. Phys. **75** (1981) 2583.
[10] D. Sengupta and J.O. Artman, J. Chem. Phys. **53** (1970) 838.
[11] C.A. Morrison and R.P. Leavitt, in: Handbook on the Physics and Chemistry of Rare Earths, Vol. 5, eds. K.A. Gschneider and L. Eyring (North-Holland, Amsterdam, 1982) p. 461.
[12] C.K. Jayasankar, M.F. Reid and F.S. Richardson, Phys. Stat. Sol. (b) **155** (1989) 559.
[13] D.R. Lide (ed.), CRC Handbook of Chemistry and Physics, 72 ed. (CRC Press Inc., Boca Raton, 1991) p. 4–121.